The Deposition and Reduction of Oxidized Mercury on the Ice Surface: Quantum-Chemical Study and Implication of Mercury Activities in the Arctic

Logan Vogelsong,[1,2] Jose D. Fuentes[3] and Abu Asaduzzaman[2,*]

[1]Department of Chemical Engineering, Pennsylvania State University, University Park, PA 16802, USA
[2]School of Science, Engineering and Technology, Pennsylvania State University – Harrisburg, Middletown, PA 17057, USA
[3]Department of Meteorology and Atmospheric Science, Pennsylvania State University, University Park, PA 16802, USA

*Email: aua1309@psu.edu

Abstract: Mercury is released into the atmosphere as atomic Hg(0) where it is oxidized under ultraviolet light to form oxidized mercury molecules as XHgY, BrHgOX, BrHgXO XHgOH, $XHgO_2H$, $XHgNO_2$, where X, and Y represent the Cl, Br, and I atoms. These gaseous oxidized mercury species (GOM) then deposit onto the surface, including on the Arctic ice and snow. The deposition and reduction mechanism of oxidized mercury on the ice surface is investigated using first-principles density functional theory (DFT). Deposition of oxidized mercury molecules is characterized by adsorption on the (0001) ice surface. Calculated adsorption energies between -2.33 and -4.33 eV confirm the strong interaction between mercury molecules and the ice surface. Further, including the thermal corrections to the total electronic energy and entropy for each mercury molecule, the Gibbs free energy of adsorption is calculated at 0 ºC. The calculated Gibbs free energy of adsorption is negative (-1.60 to -3.60 eV), which confirms the exoergic nature of adsorption processes. Further, strong interactions between ice surface and mercury molecules indicate the retention of mercury molecules on the surface and validates the previous studies on the high concentration of Hg during springtime in the Arctic. Other than BrHgOBr and BrHgOI, all molecules are dissociatively adsorbed on the surface. The dissociation of mercury molecules leads to formation of a reduced Hg atom on the surface. As the elemental mercury has low vapor pressure, low water solubility, and is weakly adsorbed on the surface, the surface reduction of mercury provides a new path for mercury reduction and reemission to the atmosphere.

Introduction

Mercury (Hg) is a dangerous neurotoxin that causes harm to developing fetuses as well as neurological damage resulting in irritability, fatigue, movement difficulties, etc.[1–4] Hg primarily enters the human body through the consumption of fish, which is especially dangerous to the indigenous people of the Arctic who use marine fish for their primary diet.[1,5]

Atmospheric transformation of mercury can play an important role in the global cycling of mercury species.[6,7] Hg is released to the environment in a variety of ways; anthropogenic sources such as the combustion of coal and small-scale gold mining,[8] and natural sources from volcanic activity[3] or re-emission from the environment in events such as forest fires[9]. While it is currently unknown the amount of Hg that is released by natural sources, it is speculated that there are about 6,000 tons of mercury available in the atmosphere.[10]

Mercury is released to the environment in two forms: its elemental form (Hg(0)), which is called gaseous elemental mercury (GEM), or its oxidized form Hg(II), that is called gaseous oxidized mercury (GOM). GOM can also bind with particles in the air to become particulate bound

mercury (PBM) that can migrate to the snow surface easier. Hg(0) stays in the atmosphere for a couple months[11] due to its lower vapor pressure, lower solubility in water, and low reactivity.[9] Long-range transport of mercury in the atmosphere is primarily in the form of Hg(0) while Hg(II) is easier to be scavenged, so it is readily deposited on the surface. Once oxidized to Hg(II), mercury becomes water soluble and more reactive[3] which allows Hg to enter the environment. The primary process for the deposition of mercury is thus the oxidation of Hg(0) to Hg(II).[12,13] The exact identity of atmospheric Hg(II) species, however, is still under investigation.[14] The inorganic Hg(II) in the aquatic environment can be converted to methylmercury (MeHg), which is then readily taken up by and is biomagnified in the food web.[7,15–19]

Hg(II) is directly released as $HgCl_2$, a by-product from coal plants. However, it deposits locally, usually within days to weeks;[20,21] while Hg(0) has the necessary lifetime to travel far away from sources. Hg can either be wet deposited by the process of precipitation mixing with GOM in the atmosphere or dry deposited from the GOM settling on the surface.[1]

To oxidize Hg(0) to Hg(II), there must be halogens (Br_2, Cl_2, I_2) present, UV light, and polyatomic radicals. UV light first photolyzes the halogen molecules, which are abundant in the Arctic environment,[22–24] to make radicals capable of reacting with Hg(0). This XHg· (X = Br, Cl, I) molecule can then either dissociate back to elemental Hg and the radical or react with another radical, halide oxide, or polyatomic molecules such as nitrogen dioxide (NO_2), hydroxyl radical (OH), and hydroperoxyl radical (HO_2).[8,11] In the springtime, the Arctic can experience 24-hour day cycles where 90% of Hg is lost from the atmosphere due to deposition on to the surface in a process known as Atmospheric Depletion Mercury Events (ADMEs).[6,12,25] The discovery of AMDEs accelerated the understanding of the Hg cycle in the polar regions. Furthermore, sea ice in the Arctic provides a semi-permeable and seasonally variable interface between water and ice for the exchange of Hg, organic compounds, halogen compounds, and heat. It also provides a habitat for food web from bacteria, algae, zooplankton, and other microorganisms to seals, beluga whales, and polar bears. During the winter months, the formation of new ice contributes brine to the ocean and helps to mix in the winter polar boundary layer and Arctic haloclines' convection. Early in the spring, halogen aerosols can be emitted from leads or polynyas (locations where upwelling water or dynamic processes maintain openings in sea ice) that develop as sea ice starts to break. When new sea ice forms, brine and frost flowers fractionate halogens and other chemical compounds, depositing them onto the sea ice surface.

However, the fate of the deposited mercury on the snow and ice surface is not well known.[7,26] It has also been observed that within 24 hours of deposition of Hg from the atmosphere, a fraction is re-emitted as a gaseous Hg(0) back to the atmosphere.[26–33] A study on the sea ice near Utqiagvik, Alaska suggests the variability in Hg concentrations increases with time.[34] Such rapid changes in Hg can be linked to the thermodynamic favorability of some Hg complexes. A variety of factors, including snow crystal type and its formation history, temperature, availability of sunlight, presence of a water layer on snow grains, and chemical compositions of snow/ice can greatly affect the retention or loss of Hg.[33] An increasing concentration of MeHg in the snowpack just before the snow melt also suggests a possible migration of mercury into the ice. Non-photo interaction of Hg with microbes and organics can also play a role in removing Hg from the atmoshere.[35–37]

Geoscientific numerical models of various complexities have been used to integrate the process-level understanding of mercury cycling in the environment[6,38] to determine the transport and chemical transformation of Hg in the atmosphere−ocean−terrestrial system. The accuracy of model representation for Hg chemistry is important for the determination of where, when, and how much Hg transformation and deposition occur over different locations across the globe. Some

models do not represent the ocean mercury chemistry explicitly but use empirical partition fractions for dissolved elemental mercury, dissolved oxidized reactive mercury ($Hg(II)_{aq}$), and particulate bound mercury.[13] Other numerical models do not include the reduction−oxidation cycle between reactive and elemental mercury but have an explicit approach for particulate bound mercury formation and transport. Saiz-Lopez et al.[20,21] showed how global mercury budget changes by considering different mercury reduction pathways although new oxidation pathway is proposed very recently.[24] On the contrary, reduction pathway of mercury is still infancy.

A detailed representation of mercury species and reactions with snow and ice surface to mimic Arctic's mercury deposition is thus the focus of the study. The study is carried out using quantum-chemical methodologies. The snow is modeled as a cluster approach and ice is modeled with the bulk ice and its surface. This study solely focuses on the reaction between oxidized mercury molecules and ice surfaces. The study is expected to answer some key questions on mercury in the Arctic surface: the deposition mechanism of oxidized mercury on the surface and role of surface on the reduction of oxidized mercury, which enable to explain the mercury budget during AMDE.

Computational Methods

All calculations were preformed applying density functional theory (DFT) using VASP (Vienna Ab initio Simulation Package), version 5.2.[39,40] The generalized gradient approximation (GGA) functional, PBE[41] and potential projected augmented wave (PAW)[40,42] were used for calculations. Different GGA functionals like AM[43–45] and PBEsol[46] were used to optimize the bulk ice. Similarly, various dispersion corrections in combination with PBE functionals were used to optimize the bulk ice. Among all the functionals and dispersion corrections, PBE functional reproduces the structural parameters of ice the best, which agree with previous studies.[47] Therefore, we used it in this study.

The (0001) surface of ice is created by cleaving an optimized bulk hexagonal-ice polymorph (Ih). A (4 × 4) supercell including four bilayers containing 256 water molecules (see Figure 1) was chosen for the calculations. The cutoff energy for the plane wave expansion is set to 500 eV, which is well above the default value and ensures convergence in calculations. Due to large supercell, the k-point sample is set to gamma point only. The convergence criteria are such that the force on each atom is equal or less than 0.02 eV/Å. The effective vacuum space above the surface is 11.36 Å. Higher vacuum spaces at 15 and 20 Å are tested for some compounds with negligible impact on the results. The atoms from the bottom layer are kept at their bulk position to mimic the bulk structure while atoms from the remaining three layers were allowed to relax. Similar methods are successfully employed in many previous adsorption studies on the ice surface.[4,37,47–50] It is to be noted that most mercury molecules are dissociated on the surface. The distances between dissociated fragments are up to 9Å. To avoid any interactions between fragments in the neighboring periodic cell, such a large 4×4 (17.76 Å ×15.44 Å) supercell is chosen.

Bader charges[51] have been calculated from the software code developed by Henkelman and co-workers.[52–54] The software utilizes the electron charge density as obtained from VASP calculations.

As reported previous studies[2], the oxidized mercury compounds included in Table S1 were tested. While some combinations have been experimentally shown,[8] all literature reported mercury molecules are explored to any possible avenues for mercury deposition to the surface. Specifically, we wanted to explore the type of molecules, which are thermodynamically stable on the ice surface

and type of molecules, which are responsible for reduction and re-emission into the atmosphere or diffusion into the bulk ice. These individual oxidized mercury compounds were optimized in a 20×20×20 Å^3 volume using the same functional, cutoff energy, k-point sampling and convergence criteria. The optimized structures of all mercury compounds, which agree with previous study[2] are shown in Table S1. Further, thermal corrections to electronic energy and entropy of all molecules are used from previous study[2].

Both parallel and perpendicular orientation of mercury molecules with respect to ice surface was investigated. The adsorption for parallel orientation is stronger than that of perpendicular orientation and results for parallel orientation, thus, is presented in the manuscript. The optimized coordinates of all mercury-ice systems are available in Table S2.

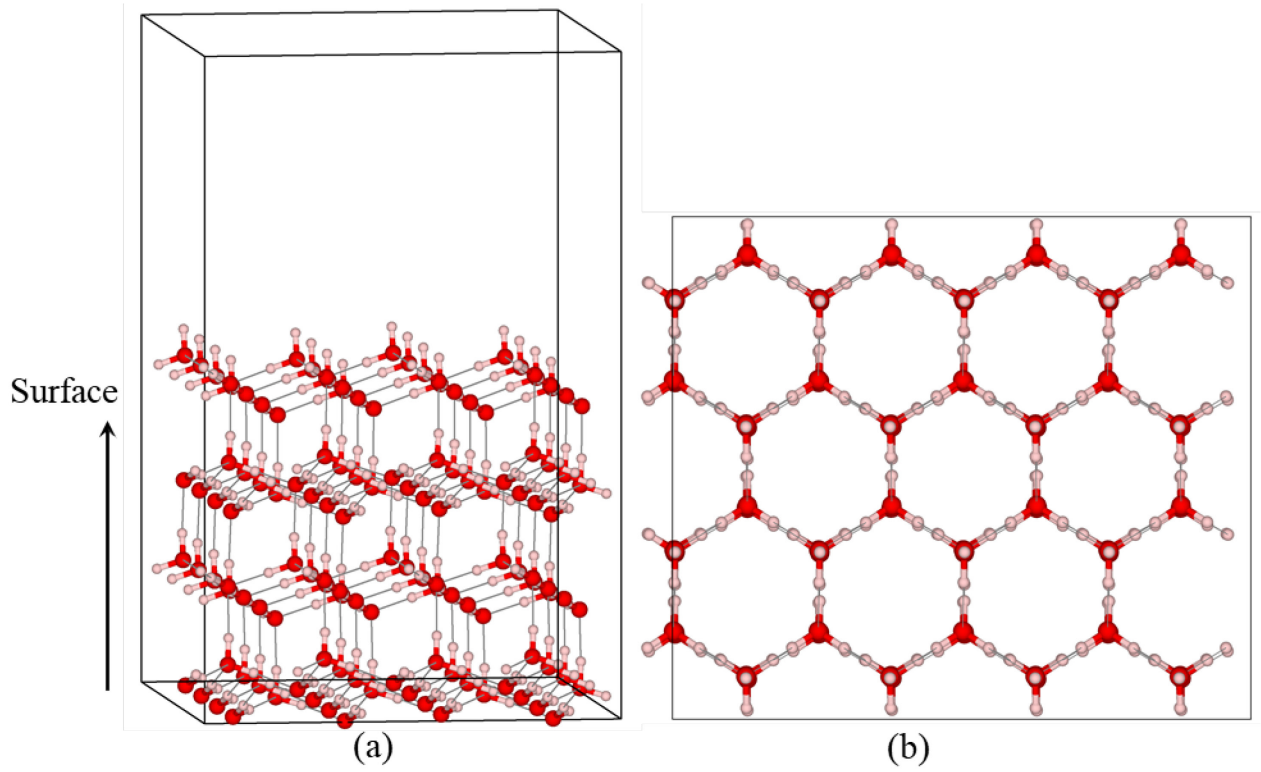

Figure 1. *Ball and stick presentation of (a) side view and (b) top view of the (0001) surface of ice. Red and white spheres represent oxygen and hydrogen atoms, respectively.*

Results and Discussion

Adsorption energies

The adsorption of oxidized mercury species on the (0001) surface of ice is explored using different initial configuration of molecules on the surface. The minimum energy configuration of adsorption is chosen in this study. Adsorption energy, ΔE_{ads}, for each oxidized mercury molecule was calculated using the following equation:

$$\Delta E_{ads} = E_{GOM\_surface} - (E_{surface} + E_{GOM}) \quad \text{.....(i)}$$

where $E_{GOM\_surface}$, $E_{surface}$ and E_{GOM} are the total energy of the adsorbed system, ice surface and corresponding mercury molecule, respectively. The negative ΔE_{ads} signifies stable adsorption.

However, for the sake of simplicity only numerical values will be used to qualitatively describe the adsorption. For example, the BrHgOBr molecule has the highest adsorption energy among all chemical species.

The adsorption energy of all molecules is negative (Table S3 and Figure 1) in response to the stable adsorption of oxidized mercury molecules on the ice surface. Further, the adsorption energies of all molecules are relatively high (3-4 eV). Such high adsorption energy confirms the strong interaction between molecules and the ice surface.

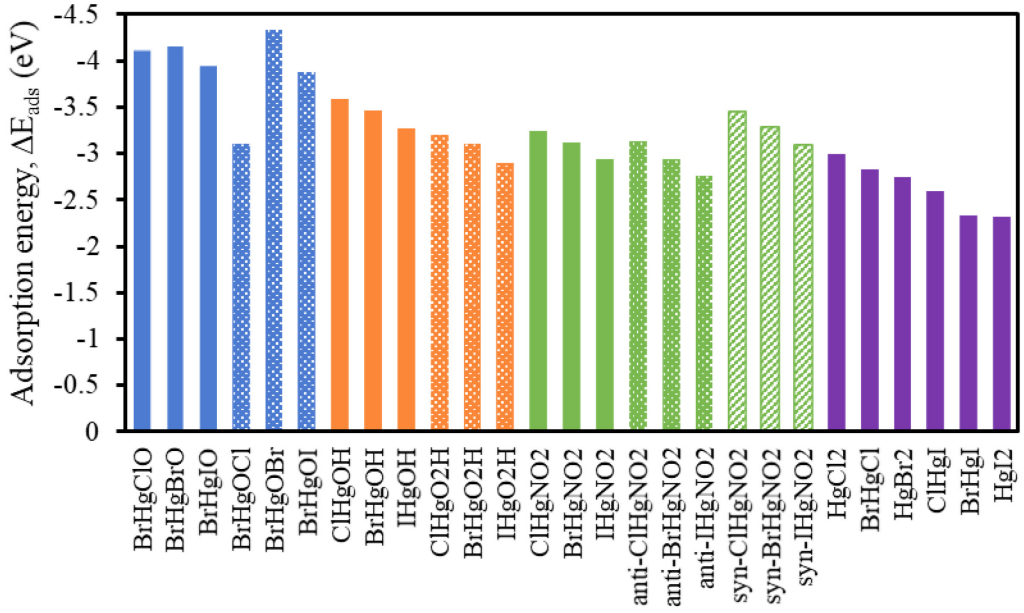

Figure 2. *Adsorption energy in eV of mercury molecules on the (0001) surface of ice. The numeric in the formula (x-axis) of molecules should be read as subscripts. For example, IHgNO2 should be read as* $IHgNO_2$.

Another important observation is that while all molecules are strongly adsorbed on the surface, certain molecules are adsorbed stronger than others. In order to quantify this effect, we have grouped all oxidized mercury molecules into four classes as was done in a previous study[2]: (a) mercury – halides (pure and mixed), (b) mercury – oxyhalides and mercury – halogen oxides, (c) mercury – hydrogen oxide and (d) mercury – nitrogen oxides. The class dependent adsorption energy is shown in Figure 3. The adsorption energy is the highest for oxyhalides whereas the same is the lowest for mixed halides. This is due the fact that the presence of OX and XO groups introduce charge separation and make those molecules more polar compared to halides. Likewise, the other important feature in adsorption energy is that for each class of molecules (except BrHgOX and BrHgXO), the adsorption energy increases from I to Br to Cl (see Figure 2). For a given class of molecules, the polar molecules or more electronegative elements exert stronger Columbic interaction with surface and therefore, resulted in higher adsorption energy. Since electronegativity increases from iodine to bromine to chlorine, the surface - halogens interactions are getting stronger, which results the highest adsorption energy for the chlorine containing molecule, whereas the lowest energy for the iodine containing molecule for a given class of molecules as can be seen in Figure 2. This observation agrees with literature report[2] on the electronic properties of those oxidized mercury molecules. The irregular trends for chlorine containing halogen oxide (BrHgClO) is due to its instability at the atmospheric conditions as

discussed by Jiao and Dibble.[8] On the other hand, the lower adsorption energy for BrHgOCl (compares to BrHgOBr and BrHgOI) is due to the resultant optimized products on the surface. Specifically, while BrHgOCl is dissociated, BrHgOBr and BrHgOI form BrHgOH type compounds on the surface.

On the other hand, adsorption energy among different classes of molecules varies with both the compositions and structures of mercury molecules and their resultant products on the surface. For example, BrHgBrO molecule dissociates to form H_2OBr and HBr type of molecules. Similarly, BrHgOBr form a BrHgOH and HBr type of molecule on the surface. It was reported that BrHgXO molecules are much unstable[2,8] than BrHgOX molecules due to the -X-O linking in the previous as opposed to -O-X linking in the latter. Therefore, the higher adsorption energy for BrHgOX/XO molecules are resulted due to the formation of -O-X linking on the surface. The adsorption energy is the lowest for the halides due to the fact that no hydrogen bond can be formed between molecules and surface. For XHgOH and $XHgO_2H$ molecules, the resultant product after the dissociation on the surface is H_2O for XHgOH as opposed to HO_2 for $XHgO_2H$ (see Figure 5). The higher stability of H_2O confirms the higher adsorption energy for XHgOH. Finally, the interactions between O atom of mercury molecules and surface H play a major role in determining the adsorption energy of nitro molecules although structural arrangement of atoms in the molecules also play a role as is seen in Figure 2 (green bars).

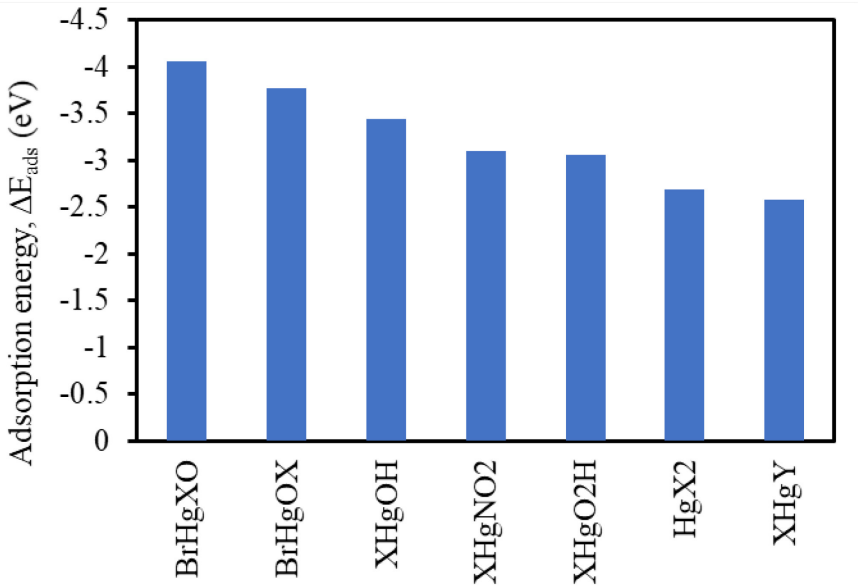

Figure 3. *Adsorption energy, ΔE_{ads} arranged by family. Adsorption energy of each class is an average of all molecules of the family. X and Y represent halogen atoms. The numeric in the formula (x-axis) of molecules should be read as subscripts. For example, HgX2 should be read as HgX_2.*

Adsorption geometries

Having found the strong adsorption energy, the focus was then turned on to analyzing the geometry of adsorbed molecules. Most of the molecules are dissociated upon reaching the surface. To illustrate the dissociation of mercury molecules on the surface, bond distances involving the Hg atom in oxidized mercury molecules in the atmosphere and on the surface are shown in Table 1. Specifically, Hg-halogens, Hg-O, and Hg-N bond distances in oxidized mercury molecules both in gas phase and on the surface are presented. Hg-surface bond in the adsorbed geometry is also presented.

The BrHgXO and BrHgOX (X = Cl, Br, and I) species (except BrHgOCl) have the highest adsorption energies among all molecules. The BrHgOCl and BrHgXO species were dissociated into Br, Hg, and OCl/XO (Figure 4a) on the surface which is seen in the bond distance between Hg-Br and Hg-XO increasing on average from 2.445 Å and 2.442 Å to 3.502 Å and 4.557 Å, respectively. The halo oxide (XO) part would abstract a surface hydrogen and form a bond with the surface (Figure 4b). Most species followed this dissociating behavior, but BrHgOBr and BrHgOI were the only ones to adsorb associatively on the surface out of all the tested GOM. The halogen atoms in oxyhalides (X in OX) behaved as leaving groups and allowed the oxygen to abstract a surface hydrogen and form bonds with the surface. The halides then travel to a vertex of the hexagonal lattice of ice (for Br) (see Figure 4b), or at the center of a hexagonal face (for I). The Br-Hg bond distance increased by 0.038 Å on average and the Hg-O decreased by 0.040 Å on average. These small bond distance changes show the overall compound shape was retained. The surface adsorbed the newly formed oxidized BrHgOH (Figure 4b).

Table 1. Bond distances in Å between Hg and electronegative atoms in oxidized mercury molecules both in gas phase (in the atmosphere) and on the surface. The X is the left atom, and the Y is the right atom bonded to Hg, as given by the molecule column. The Hg-surface bond distance is presented by the distance between Hg and the closest surface H.

Molecules	In atmosphere (d_{atom})		On surface (d_{surf})		$\Delta d = d_{atom} - d_{surf}$		$Hg\text{-}H_{surf}$
	X-Hg	Hg-Y	X-Hg	Hg-Y	X-Hg	Y-Hg	
$HgCl_2$	2.282	2.282	4.934	4.807	2.652	2.525	2.636
$HgBr_2$	2.425	2.425	4.105	5.399	1.680	2.974	2.623
HgI_2	2.604	2.604	3.544	5.398	0.940	2.794	2.646
BrHgCl	2.416	2.294	3.814	7.140	1.398	4.845	2.010
BrHgI	2.438	2.590	3.287	6.700	0.850	4.111	2.290
ClHgI	2.308	2.584	3.478	6.946	1.170	4.362	2.564
BrHgClO	2.450	2.447	3.445	5.070	0.995	2.622	2.726
BrHgBrO	2.454	2.563	3.430	5.081	0.976	2.518	2.723
BrHgIO	2.460	2.703	3.461	4.842	1.001	2.139	2.706
BrHgOCl	2.411	2.053	3.673	3.234	1.263	1.181	3.441
BrHgOBr	2.411	2.044	2.457	2.005	0.047	-0.039	3.405
BrHgOI	2.412	2.039	2.442	1.997	0.030	-0.0419	3.221
ClHgOH	2.280	2.008	3.498	4.935	1.217	2.928	2.647
BrHgOH	2.412	2.017	3.350	4.836	0.937	2.819	2.652
IHgOH	2.575	2.029	3.428	4.555	0.853	2.526	2.720
$ClHgO_2H$	2.282	2.024	3.856	3.477	1.574	1.453	3.537
$BrHgO_2H$	2.414	2.036	3.782	3.351	1.368	1.314	3.454

$IHgO_2H$	2.581	2.046	3.634	3.298	1.053	1.252	3.468
$ClHgNO_2$	2.306	2.168	4.450	3.876	2.144	1.709	2.637
$BrHgNO_2$	2.437	2.174	4.179	3.849	1.742	1.676	2.648
$IHgNO_2$	2.601	2.202	3.756	3.821	1.156	1.619	2.664
anti-ClHgONO	2.276	2.043	4.473	4.514	2.197	2.471	2.663
anti-BrHgONO	2.407	2.058	4.293	4.464	1.885	2.407	2.659
anti-IHgONO	2.576	2.071	3.785	4.606	1.210	2.536	2.691
syn-ClHgONO	2.303	2.179	4.154	3.527	1.851	1.348	3.425
syn-BrHgONO	2.421	2.200	3.881	3.559	1.460	1.359	3.436
syn-IHgONO	2.606	2.255	3.768	3.484	1.161	1.230	3.392

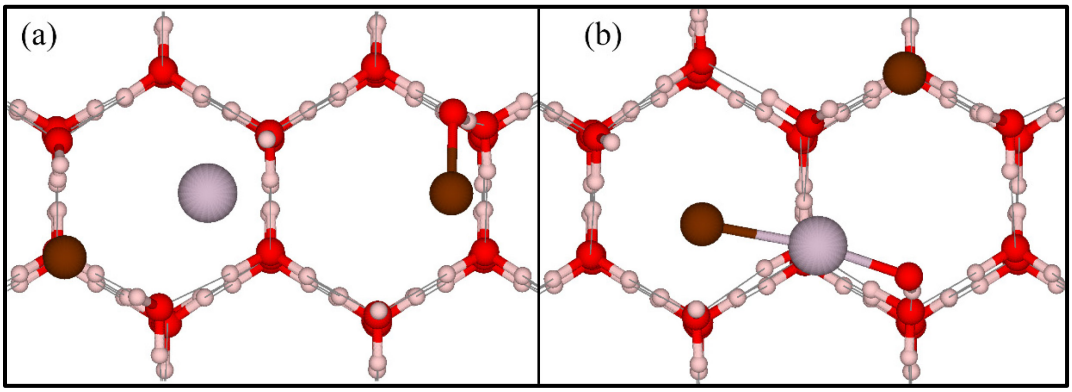

Figure 4. *Top view of the adsorbed structure of (a) BrHgBrO and (b) BrHgOBr on the (0001) surface of ice. BrHgBrO has dissociated into pieces while BrHgOBr becomes BrHgOH on the surface. The gray and brown spheres represent Hg and Br atoms, respectively. The other presentation is as of Fig. 1.*

XHgOH molecules have the second highest adsorption energy on the ice surface. All three of these molecules showed similar geometries regardless of halide type. They would break into three parts: the halide, Hg, and a H_2O formed with a surface hydrogen (Figure 5a). Hg-$H_{surface}$ bond distance on average was 2.673 Å and X-Hg distanced increased by 1.003 Å and Hg-Y increased by 2.758 Å.

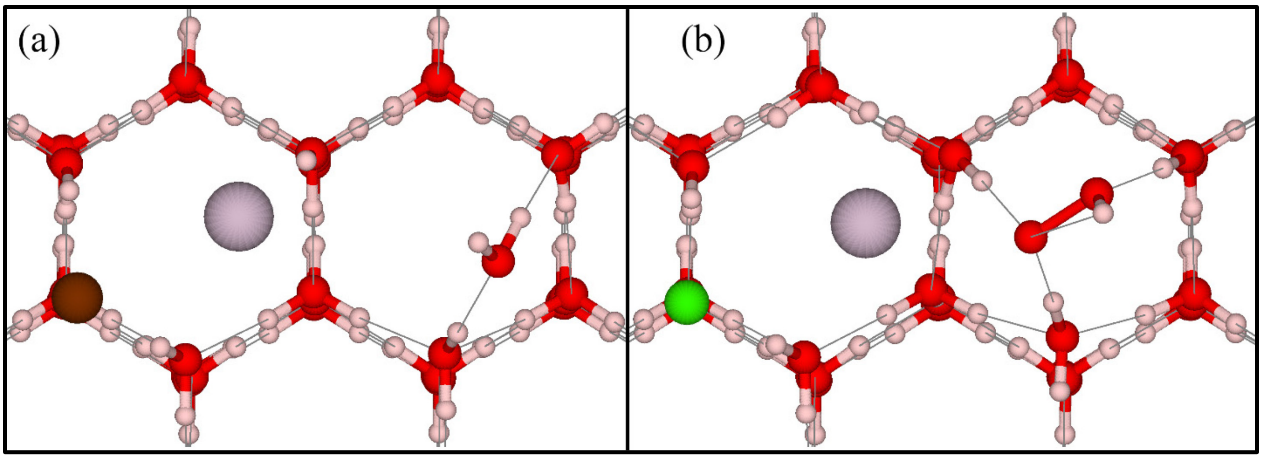

Figure 5. *Top view of the adsorption structure of (a) BrHgOH and (b) ClHgO$_2$H on ice surface. The presentation is as of Figure 1 and 4.*

The XHgO$_2$H broke into three pieces like the other compounds: the halide, Hg, and OOH group. X-Hg distances increased on average by 1.332 Å and Hg-OOH increased by 1.340 Å after dissociation. The OOH group formed bonds with each of their oxygen atoms to different hydrogen atoms in the middle of the supercell. They did not abstract a surface hydrogen to make a peroxide from the dissociated OOH group. The Hg atom was 3.486 Å away from a surface hydrogen (Figure 5b).

Next, nine nitro species with different structure were adsorbed on the surface. The *syn*-conformer has been shown to be the most stable[5] and all three *syn*-conformers have, on average, higher adsorption energy than the XHgNO$_2$ conformers, which have subsequently higher adsorption energy than the *anti*-conformers. Chlorine containing molecules formed the strongest bond to the surface followed by bromine and then iodine which can be explained from the electronegativity order of halogens. Chlorine also traveled the furthest away out of all the halides and iodine traveled the least. All three conformers broke into three parts: the halide, Hg, and NO$_2$. From all these species, on average, the halide-Hg bond increased by 1.645 Å and the Hg-Y bond increased by 1.817 Å. Both the XHgNO$_2$ conformer and *anti*-conformers' nitro group bonded to the same surface hydrogen (Figure 6b) whereas the *syn*-conformer's nitro group hydrogen bonded to the surface H closest to the original position of Hg (Figure 6a). This shifted the Hg away from the surface hydrogen, allowing a much higher adsorption energy (Figure 6a). The average Hg-H$_{surface}$ bond distance was also greater for *syn*-conformers at 3.418 Å versus for *anti* and XHgNO$_2$ at 2.660 Å.

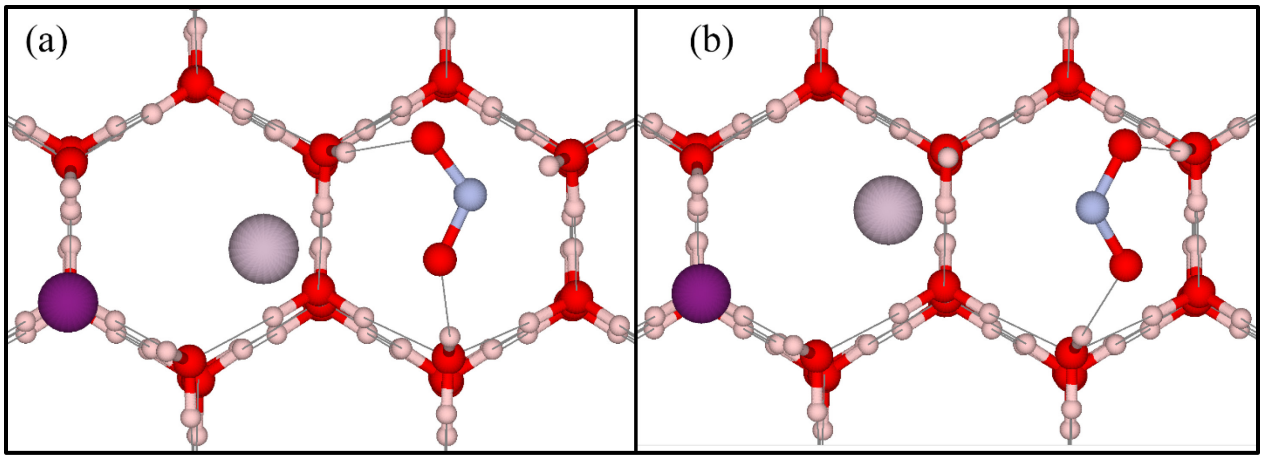

Figure 6. *Top view of the adsorption structures of (a) syn-IHgNO$_2$ and (b) anti-IHgNO$_2$ on ice surface. Blue and purple sphere represent nitrogen and iodine atoms, respectively. All other representation is as of Figure 1 and 4.*

Finally, the last two halide-only species were the weakest to interact, but they still showed spontaneous dissociation on surface. Even though their structure is halide-Hg-halide, their resulting geometries on the surface are different and shown in Figure 7. The resulting Hg in XHgY species was the closest to the surface out of all molecules. Hg-H$_{surface}$ distance was 2.318 Å on average for the XHgY family. The Hg atoms were optimized in the middle of a hexagonal opening of ice. Bond distances of XHgY on average increased 1.139 Å (X-Hg) and 4.439 Å (Hg-Y), respectively. HgX$_2$ bond distances increased 1.757 Å (left side X-Hg) and 2.764 Å (right side Hg-X) from gaseous to surface. The Hg-H$_{surface}$ bond distances are some of lowest recorded at 2.318 Å for XHgY and 2.635 Å for HgX$_2$. In both cases, the halogen atoms move on top of surface oxygen atom where the nearby hydrogen atoms stabilized it. However, the Hg in XHgY would be stabilized by the surface hydrogen atoms (Figure 7b) instead of both halides in HgX$_2$; the X in XHgY would settle above the oxygen with a hydrogen (Figure 7a).

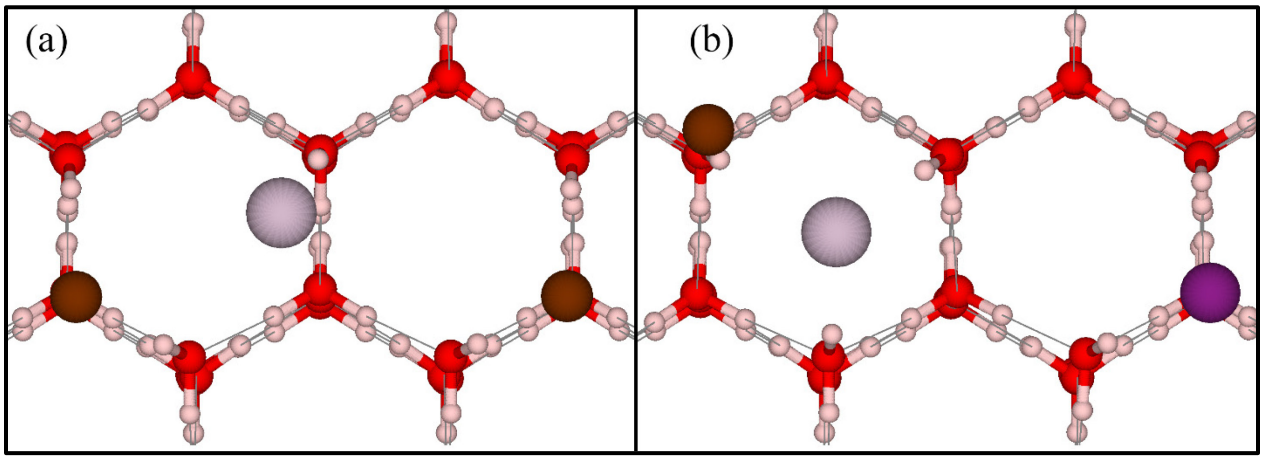

Figure 7. *Top view of the adsorption structure of (a) HgBr$_2$ and (b) BrHgI. The presentation is as of Figure 1 and 3.*

Bader charges on Hg

The dissociation of GOM is expected to impact the oxidation state of Hg. Oxidation state of Hg is analyzed by calculating the Bader charge on Hg in both gaseous mercury molecules and on the surface. Note that Bader charge is calculated by integrating the electron density around an atom in a given molecule, which more often is a fractional number and not the oxidation state of the atom.[2] However, it is an important tool when Bader charge analysis is compared with a known standard.

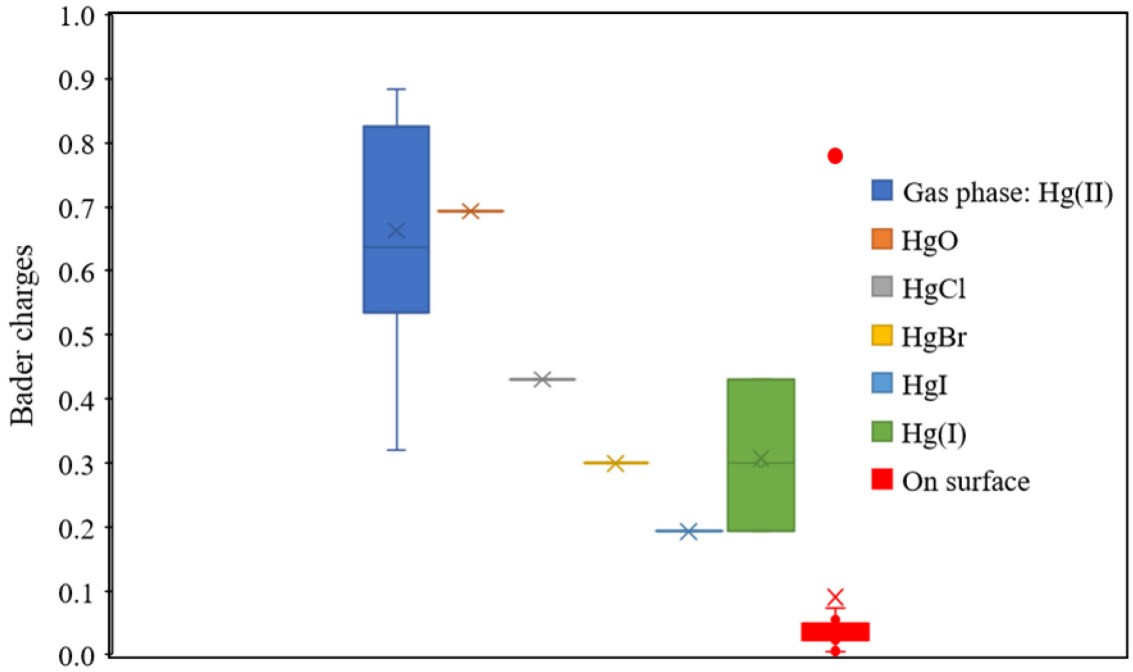

Figure 8. *Box and whisker plot for the Bader charges on Hg atom in oxidized mercury molecules both in gas phase and on surface. Bader charges on Hg in few molecular species are also shown.*

In our case, comparing the Bader charges on Hg atom in gas phase with the one on the surface will provide significant information of the oxidation-reduction of Hg due the adsorption. The Bader charge on Hg in both gas phase and on surface, and the reduction of charge from gas to surface is shown in Table S4. Similarly, Bader charge on Hg in HgX (X = Cl, Br, I) and HgO along with box and whisker plot for those in oxidized mercury molecules are presented in Figure 8 and 9.

In agreement with a previous study[2], the charges on Hg in oxidized mercury molecules depend on the connecting anions (HgCl, HgBr, HgI in Figure 8): higher the negativity of anions, higher the charge on Hg. Additionally, the charge on mercury in all gas phase molecules is similar as of HgO, where the oxidation state of Hg is 2+. Another important observation is that although Bader charge on Hg depends on connecting anions, it follows the regular pattern for same anions. For example, the Bader charge on Hg in $HgCl_2$ and HgCl are 0.86 and 0.43, respectively, which is consistent with the oxidation states of 2+ and 1+, respectively. This consistency lays the foundation of deducing reduction state of Hg on ice surfaces.

Now, comparing the Bader charges on Hg in oxidized mercury molecules in gas phase with the ones on the surface, both as a box and whisker plot (Figure 8) and individual class (Figure 9a), other than BrHgOX class, the Hg atom is highly reduced on the surface. The extent of reduction in individual molecule is further visible in Figure 9b and Table S4. Also, there is a direct correlation between the dissociating molecules on the surface and reduced state of Hg: Hg in

surface dissociated molecules is greatly reduced. It is plausible that the surface play an important role in reducing Hg upon adsorption. Depending on the structural commensuration of molecules with surface structures, the anion parts of molecules interact with the surface hydrogen and oxygen and form O-H bond. At the same time, Hg lost its binding connection from the anions and get reduced.

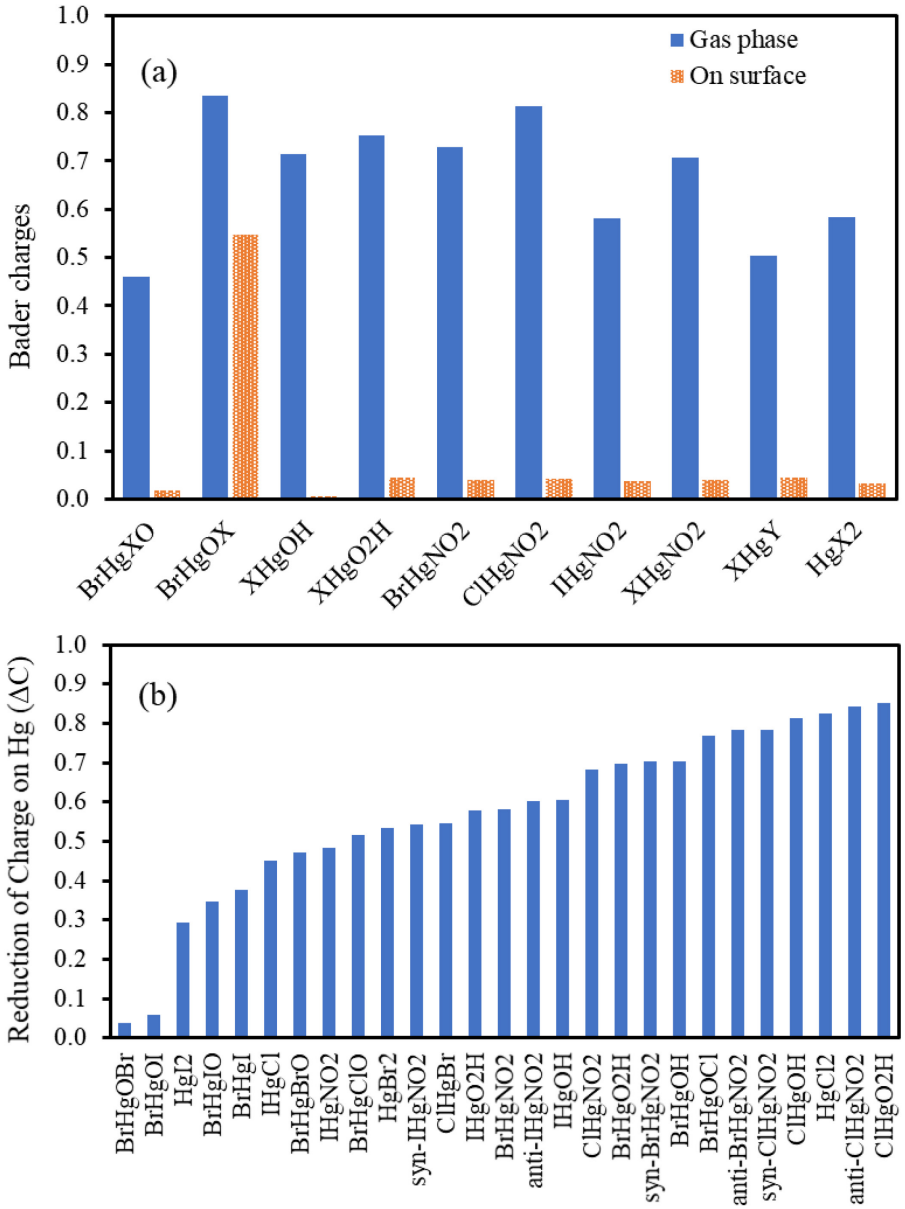

Figure 9. *(a) The average Bader charges on Hg atom both in gas phase and on surface are classified as family. (b) The reduction of charge on mercury from gas phase to surface for each molecule. The numeric in the formula (x-axis) of molecules should be read as subscripts. For example, ClHgO2H should be read as* $ClHgO_2H$.

Stability of mercury molecules on the ice surface

The adsorption energy of mercury molecules was calculated at 0 K (-273 ºC), which is standard for DFT methodologies. However, the temperature in the Arctic is between 233K to 263K during the winter time. Therefore, temperature effect on the stability of mercury molecules has been investigated under temperature lower than the ambient conditions. Thermal corrections to the total electronic energy (E_t) and entropic contributions (S) are the two temperature dependent factors that controls thermodynamic stability of a given process. Since structures of surface do not change significantly, it is fair to assume that change of thermal corrections to electronic energy ($\Delta E_{t\text{-}surf}$) and entropy (ΔS_{surf}) from bare and adsorbed surface is zero. Thus, the thermal corrections to energy and entropy of mercury molecules are the only temperature dependent contribution to the adsorption process. On the adsorbed surface, the rotational and translational degree of freedoms of mercury molecule are restricted., leaving the vibrational degree of freedom is the only temperature dependent contributor, which is small below 0 ºC. Finally, the Gibbs free energy of adsorption ($\Delta G_{0\text{-}ads}$) is calculated at 0 ºC by including the thermal correction to the electronic energy ($E_{0\text{-}mol}$) and entropy ($S_{0\text{-}mol}$) of gas phase mercury molecules:

$$\Delta G_{0-ads} = \Delta E_{ads} - E_{0-mol} - S_{0-mol} \quad \text{.....(ii)}$$

It is to be noted that thermal corrections and entropic contributions from adsorbed molecules will have more negative $\Delta G_{0\text{-}ads}$. Similarly, $\Delta G_{0\text{-}ads}$ will be more negative for temperature lower than 0 ºC. Further, more negative adsorption free energy signifies more stability of adsorbed mercury molecules on ice surface.

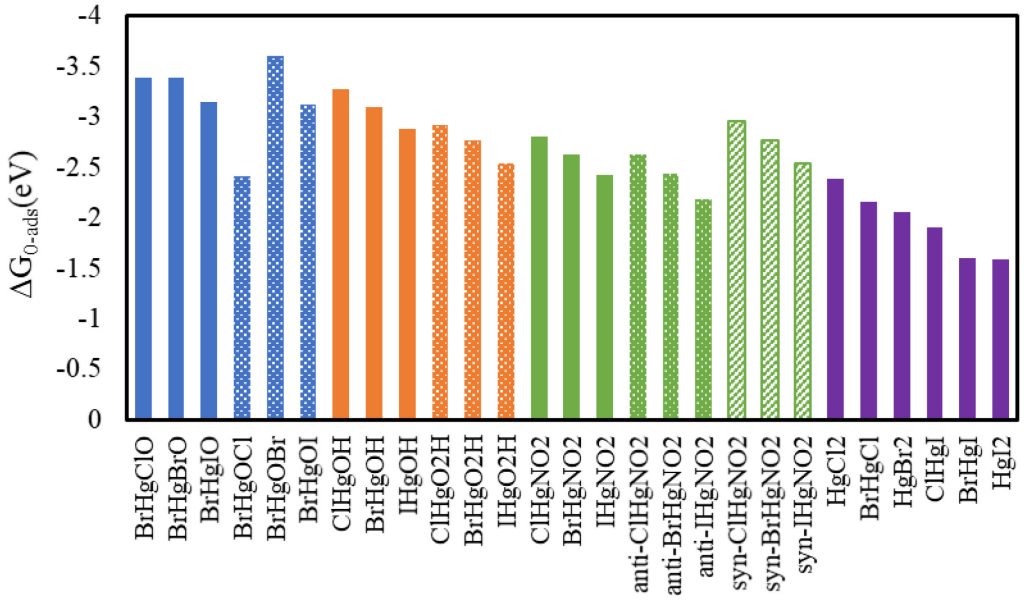

Figure 10. *The Gibbs free energy of adsorption of mercury molecules on the (0001) surface of ice. The numeric in the formula (x-axis) of molecules should be read as subscripts. For example, HgI2 should be read as* HgI_2.

It is clear from the Figure 10 that Gibbs free energy of adsorption of all molecules is -1.6 to -3.6 eV, which are well below zero eV at 0 ºC. Such negative adsorption free energy confirms the stability of adsorbed molecules on the ice surface. Any temperature lower than 0 ºC will only enhance the stability of molecules on the surface.

Implication of Hg deposition and reduction in the Arctic

Oxidation-reduction of Hg is a complex phenomenon in the global mercury cycle. While photo induced oxidation of Hg is a well-studied area, the reduction of Hg is not. Recently, a couple of studies devoted on elucidating the reduction mechanism by calculating an optical cross section of mercury molecules.[20,21] Until the discovery of AMDEs, the drastic oxidation of mercury in the Arctic was a rather perplexing question. Discovery of AMDEs provided a plausible explanation of the photo oxidation of Hg due to the 24 hours of sunlight following the polar sunrise. After oxidation of mercury, the oxidized mercury molecules deposit on the surface, i.e., on ice and snow surface. Field measurements[26,34] also reported that a majority of surface deposited mercury reduce back to the atmosphere during AMDEs. The reduction of deposited mercury was inferred from the measurement of deposited mercury, which was much less than the initial deposition. However, neither deposition nor reduction was characterized by experimental or computational studies. To our knowledge, this is the first study to characterize the deposition of oxidized mercury molecules at the atomic scale and provide a plausible route for reduction of deposited mercury. All oxidized mercury molecules are strongly adsorbed on the ice surface: adsorption energy is in the range of -2.33 to -4.33 eV. Such high adsorption energy confirms strong chemical interaction between molecules and surface. Further, the Gibbs free energy of adsorption suggest the strong thermodynamic favorability of adsorption at 0 ºC. At the subzero temperature in the Arctic (-10 to -40 ºC), the probability of desorption of oxidized mercury molecules is, thus, low. This validates the measurement on drastic decreases of Hg in the atmosphere during the springtime. It can also be extended that as soon as mercury molecules are formed in the atmosphere in the Arctic or Antarctic, they will deposit onto the surface and bind strongly with the ice surface.

The other important implication is the reduction of mercury after deposition. Our calculations showed that Hg in most molecular forms is reduced to almost atomic Hg on the surface. As shown in the previous study,[47] Hg atoms interact with the surface through weak van der Waal's forces. Such a weakly bonded, reduced mercury atom likely return to the atmosphere. On the other hand, in those mercury-containing molecules where mercury atoms stay oxidized, mercury ions will diffuse through the ice and/or through brine channel to reach the aquatic environment where mercury bioaccumulation can occur.

Conclusions

Deposition and reduction of mercury molecules on the ice (0001) surface are carried out using a quantum-chemical methodology. Mercury molecules with a variety of anions: halides, oxyhalides, haloxides, nitro, etc. and structure: *syn*- and *anti*- are considered as adsorbates. The calculations showed that all molecules are strongly adsorbed (adsorption energy is -2.33 to -4.33 eV) on the ice surface. Such high adsorption energy hints the stability of adsorbed molecules on the ice surface. Further, after the incorporation of thermal and entropic contribution of adsorbed molecules, it is confirmed that the adsorption process is strongly thermodynamically favorable process at 0 ºC, which is well above the Arctic temperature. Consequently, any temperature lower than 0 ºC will only increase the thermodynamic favorability of the adsorption process. The oxidized mercury compounds tend to bond more strongly to the surface with the hydrogen as opposed to interacting with the heavier halogens. The structural analysis of adsorbed molecules reveals that most of the adsorbed molecules are dissociated on the surface. The dissociated molecules split into three parts on the surface: the halide(s), Hg, and haloxide or OX, hydroxy, nitro, OOH. The splitting of molecules reduces the Hg into the Hg(0) atom. The compounds BrHgOBr and BrHgOI are adsorbed to the surface and subsequently remained oxidized. The deposition of oxidized mercury compounds to the Arctic surface and subsequent reduction to the Hg atom allow for a possible

mechanism of mercury reduction. On the other hand, the undissociated mercury molecules on the surface provide the needed source of mercury retention during AMDEs and a possible source for mercury diffusion and methylmercury. These results show favorable mercury interactions on the Arctic ice and can improve understanding of the global mercury budget.

Supporting Information

Optimized structures of mercury molecules (Table S1), optimized coordinates (VASP POSCAR) for all adsorbed mercury molecules on ice surface (Table S2), adsorption energy (Table S3) and Bader charge (Table S4) are available in the supporting information.

Acknowledgements

This work is supported by National Science Foundation under the grant number CHE - 2137662. Computations for this research were performed on the Pennsylvania State University's Institute for Computational and Data Sciences' Roar supercomputer and at the High-Performance Computing, University of Arizona (UA HPC).

References

(1) Driscoll, C. T.; Mason, R. P.; Chan, H. M.; Jacob, D. J.; Pirrone, N. Mercury as a Global Pollutant: Sources, Pathways, and Effects. *Environ. Sci. Technol.* **2013**, *47* (10), 4967–4983. DOI: 10.1021/es305071v.

(2) Amin, S.; Asif, T.; Khan, M.; Usinowicz, E.; Mitra, D.; Asaduzzaman, A. Structural, Energetic and Vibrational Properties of Oxidized Mercury in the Gas and Aqueous Phases. *Computat. Theor. Chem.* **2021**, *1198*, 113186. DOI: 10.1016/j.comptc.2021.113186.

(3) Lyman, S. N.; Cheng, I.; Gratz, L. E.; Weiss-Penzias, P.; Zhang, L. An Updated Review of Atmospheric Mercury. *Sci. Total Environ.* **2020**, *707*, 135575. DOI: 10.1016/j.scitotenv.2019.135575.

(4) Asaduzzaman, A.; Riccardi, D.; Afaneh, A. T.; Cooper, S. J.; Smith, J. C.; Wang, F.; Parks, J. M.; Schreckenbach, G. Environmental Mercury Chemistry – In Silico. *Acc. Chem. Res.* **2019**, *52* (2), 379–388. DOI: 10.1021/acs.accounts.8b00454.

(5) Lockhart, W. L.; Stern, G. A.; Low, G.; Hendzel, M.; Boila, G.; Roach, P.; Evans, M. S.; Billeck, B. N.; DeLaronde, J.; Friesen, S.; Kidd, K.; Atkins, S.; Muir, D. C. G.; Stoddart, M.; Stephens, G.; Stephenson, S.; Harbicht, S.; Snowshoe, N.; Grey, B.; Thompson, S.; DeGraff, N. A History of Total Mercury in Edible Muscle of Fish from Lakes in Northern Canada. *Sci. Total Environ.* **2005**, *351–352*, 427–463. DOI: 10.1016/j.scitotenv.2004.11.027.

(6) Angot, H.; Dastoor, A.; De Simone, F.; Gårdfeldt, K.; Gencarelli, C. N.; Hedgecock, I. M.; Langer, S.; Magand, O.; Mastromonaco, M. N.; Nordstrøm, C.; Pfaffhuber, K. A.; Pirrone, N.; Ryjkov, A.; Selin, N. E.; Skov, H.; Song, S.; Sprovieri, F.; Steffen, A.; Toyota, K.; Travnikov, O.; Yang, X.; Dommergue, A. Chemical Cycling and Deposition of Atmospheric Mercury in Polar Regions:Review of Recent Measurements and Comparison with Models. *Atmos. Chem. Phys.* **2016**, *16* (16), 10735–10763. DOI: 10.5194/acp-16-10735-2016.

(7) Douglas, T. A.; Loseto, L. L.; Macdonald, R. W.; Outridge, P.; Dommergue, A.; Poulain, A.; Amyot, M.; Barkay, T.; Berg, T.; Chételat, J.; Constant, P.; Evans, M.; Ferrari, C.; Gantner, N.; Johnson, M. S.; Kirk, J.; Kroer, N.; Larose, C.; Lean, D.; Nielsen, T. G.;

Poissant, L.; Rognerud, S.; Skov, H.; Sørensen, S.; Wang, F.; Wilson, S.; Zdanowicz, C. M. The Fate of Mercury in Arctic Terrestrial and Aquatic Ecosystems, a Review. *Environ. Chem.* **2012**, *9* (4), 321-325. DOI: 10.1071/EN11140.

(8) Jiao, Y.; Dibble, T. S. Structures, Vibrational Frequencies, and Bond Energies of the BrHgOX and BrHgXO Species Formed in Atmospheric Mercury Depletion Events. *J. Phys. Chem. A* **2017**, *121* (41), 7976–7985. DOI: 10.1021/acs.jpca.7b06829.

(9) Ariya, P. A.; Amyot, M.; Dastoor, A.; Deeds, D.; Feinberg, A.; Kos, G.; Poulain, A.; Ryjkov, A.; Semeniuk, K.; Subir, M.; Toyota, K. Mercury Physicochemical and Biogeochemical Transformation in the Atmosphere and at Atmospheric Interfaces: A Review and Future Directions. *Chem. Rev.* **2015**, *115* (10), 3760–3802. DOI: 10.1021/cr500667e.

(10) UNEP. Chemicals and Water, Global Mercury Assessment, 2002. https://www.unep.org/resources/report/global-mercury-assessment-2002-0. (accessed on 2021-5-12)

(11) Horowitz, H. M.; Jacob, D. J.; Zhang, Y.; Dibble, T. S.; Slemr, F.; Amos, H. M.; Schmidt, J. A.; Corbitt, E. S.; Marais, E. A.; Sunderland, E. M. A New Mechanism for Atmospheric Mercury Redox Chemistry: Implications for the Global Mercury Budget. *Atmos. Chem. Phys.* **2017**, *17* (10), 6353–6371. DOI: 10.5194/acp-17-6353-2017.

(12) Steffen, A.; Douglas, T.; Amyot, M.; Ariya, P.; Aspmo, K.; Berg, T.; Bottenheim, J.; Brooks, S.; Cobbett, F.; Dastoor, A.; Dommergue, A.; Ebinghaus, R.; Ferrari, C.; Gardfeldt, K.; Goodsite, M. E.; Lean, D.; Poulain, A. J.; Scherz, C.; Skov, H.; Sommar, J.; Temme, C. A Synthesis of Atmospheric Mercury Depletion Event Chemistry in the Atmosphere and Snow. *Atmos. Chem. Phys.* **2008**, *8* (6), 1445–1482. DOI: 10.5194/acp-8-1445-2008.

(13) Strode, S. A.; Jaeglé, L.; Selin, N. E.; Jacob, D. J.; Park, R. J.; Yantosca, R. M.; Mason, R. P.; Slemr, F. Air-Sea Exchange in the Global Mercury Cycle: Mercury Air-Sea Exchange. *Global Biogeochem. Cycles* **2007**, *21*, GB1017. DOI: 10.1029/2006GB002766.

(14) Lalonde, J. D.; Poulain, A. J.; Amyot, M. The Role of Mercury Redox Reactions in Snow on Snow-to-Air Mercury Transfer. *Environ. Sci. Technol.* **2002**, *36* (2), 174–178. DOI: 10.1021/es010786g.

(15) Gionfriddo, C. M.; Tate, M. T.; Wick, R. R.; Schultz, M. B.; Zemla, A.; Thelen, M. P.; Schofield, R.; Krabbenhoft, D. P.; Holt, K. E.; Moreau, J. W. Microbial Mercury Methylation in Antarctic Sea Ice. *Nat. Microbiol.* **2016**, *1* (10), 16127. DOI: 10.1038/nmicrobiol.2016.127.

(16) Beattie, S. A.; Armstrong, D.; Chaulk, A.; Comte, J.; Gosselin, M.; Wang, F. Total and Methylated Mercury in Arctic Multiyear Sea Ice. *Environ. Sci. Technol.* **2014**, *48* (10), 5575–5582. DOI: 10.1021/es5008033.

(17) Lehnherr, I.; St. Louis, V. L.; Hintelmann, H.; Kirk, J. L. Methylation of Inorganic Mercury in Polar Marine Waters. *Nat. Geosci.* **2011**, *4* (5), 298–302. DOI: 10.1038/ngeo1134.

(18) Whalin, L.; Kim, E.-H.; Mason, R. Factors Influencing the Oxidation, Reduction, Methylation and Demethylation of Mercury Species in Coastal Waters. *Marine Chem.* **2007**, *107* (3), 278–294. DOI: 10.1016/j.marchem.2007.04.002.

(19) Zhang, Y.; Soerensen, A. L.; Schartup, A. T.; Sunderland, E. M. A Global Model for Methylmercury Formation and Uptake at the Base of Marine Food Webs. *Global Biogeochem. Cycles* **2020**, *34*, e2019GB006348. DOI: 10.1029/2019GB006348.

(20) Saiz-Lopez, A.; Sitkiewicz, S. P.; Roca-Sanjuán, D.; Oliva-Enrich, J. M.; Dávalos, J. Z.; Notario, R.; Jiskra, M.; Xu, Y.; Wang, F.; Thackray, C. P.; Sunderland, E. M.; Jacob, D. J.; Travnikov, O.; Cuevas, C. A.; Acuña, A. U.; Rivero, D.; Plane, J. M. C.; Kinnison, D. E.; Sonke, J. E. Photoreduction of Gaseous Oxidized Mercury Changes Global Atmospheric Mercury Speciation, Transport and Deposition. *Nat. Commun.* **2018**, *9* (1), 4796. DOI: 10.1038/s41467-018-07075-3.

(21) Saiz-Lopez, A.; Travnikov, O.; Sonke, J. E.; Thackray, C. P.; Jacob, D. J.; Carmona-García, J.; Francés-Monerris, A.; Roca-Sanjuán, D.; Acuña, A. U.; Dávalos, J. Z.; Cuevas, C. A.; Jiskra, M.; Wang, F.; Bieser, J.; Plane, J. M. C.; Francisco, J. S. Photochemistry of Oxidized Hg(I) and Hg(II) Species Suggests Missing Mercury Oxidation in the Troposphere. *Proc. Natl. Acad. Sci. USA* **2020**, *117* (49), 30949-30956. DOI: 10.1073/pnas.1922486117.

(22) Raso, A. R. W.; Custard, K. D.; May, N. W.; Tanner, D.; Newburn, M. K.; Walker, L.; Moore, R. J.; Huey, L. G.; Alexander, L.; Shepson, P. B.; Pratt, K. A. Active Molecular Iodine Photochemistry in the Arctic. *Proc. Natl. Acad. Sci. USA* **2017**, *114* (38), 10053–10058. DOI: 10.1073/pnas.1702803114.

(23) McNamara, S. M.; Garner, N. M.; Wang, S.; Raso, A. R. W.; Thanekar, S.; Barget, A. J.; Fuentes, J. D.; Shepson, P. B.; Pratt, K. A. Bromine Chloride in the Coastal Arctic: Diel Patterns and Production Mechanisms. *ACS Earth Space Chem.* **2020**, *4* (4), 620–630. DOI: 10.1021/acsearthspacechem.0c00021.

(24) Castro, P. J.; Kellö, V.; Cernušák, I.; Dibble, T. S. Together, Not Separately, OH and O_3 Oxidize $Hg^{(0)}$ to $Hg^{(II)}$ in the Atmosphere. *J. Phys. Chem. A* **2022**, *126* (44), 8266-8279. DOI: 10.1021/acs.jpca.2c04364.

(25) Schroeder, W. H.; Anlauf, K. G.; Barrie, L. A.; Lu, J. Y.; Steffen, A.; Schneeberger, D. R.; Berg, T. Arctic Springtime Depletion of Mercury. *Nature* **1998**, *394* (6691), 331–332. DOI: 10.1038/28530.

(26) Johnson, K. P.; Blum, J. D.; Keeler, G. J.; Douglas, T. A. Investigation of the Deposition and Emission of Mercury in Arctic Snow during an Atmospheric Mercury Depletion Event. *J. Geophys. Res.* **2008**, *113*, D17304. DOI: 10.1029/2008JD009893.

(27) Dommergue, A.; Ferrari, C. P.; Poissant, L.; Gauchard, P.-A.; Boutron, C. F. Diurnal Cycles of Gaseous Mercury within the Snowpack at Kuujjuarapik/Whapmagoostui, Québec, Canada. *Environ. Sci. Technol.* **2003**, *37* (15), 3289–3297. DOI: 10.1021/es026242b.

(28) Sherman, L. S.; Blum, J. D.; Johnson, K. P.; Keeler, G. J.; Barres, J. A.; Douglas, T. A. Mass-Independent Fractionation of Mercury Isotopes in Arctic Snow Driven by Sunlight. *Nat. Geosci.* **2010**, *3* (3), 173–177. DOI: 10.1038/ngeo758.

(29) Steen, A. O.; Berg, T.; Dastoor, A. P.; Durnford, D. A.; Hole, L. R.; Pfaffhuber, K. A. Dynamic Exchange of Gaseous Elemental Mercury during Polar Night and Day. *Atmos. Environ.* **2009**, *43* (35), 5604–5610. DOI: 10.1016/j.atmosenv.2009.07.069.

(30) Kirk, J. L.; St. Louis, V. L.; Hintelmann, H.; Lehnherr, I.; Else, B.; Poissant, L. Methylated Mercury Species in Marine Waters of the Canadian High and Sub Arctic. *Environ. Sci. Technol.* **2008**, *42* (22), 8367–8373. DOI: 10.1021/es801635m.

(31) Carignan, J.; Sonke, J. The Effect of Atmospheric Mercury Depletion Events on the Net Deposition Flux around Hudson Bay, Canada. *Atmos. Environ.* **2010**, *44* (35), 4372–4379. DOI: 10.1016/j.atmosenv.2010.07.052.

(32) Brooks, S. B.; Saiz-Lopez, A.; Skov, H.; Lindberg, S. E.; Plane, J. M. C.; Goodsite, M. E. The Mass Balance of Mercury in the Springtime Arctic Environment. *Geophys. Res. Lett.* **2006**, *33* (13), L13812. DOI: 10.1029/2005GL025525.
(33) Douglas, T. A.; Sturm, M.; Simpson, W. R.; Blum, J. D.; Alvarez-Aviles, L.; Keeler, G. J.; Perovich, D. K.; Biswas, A.; Johnson, K. Influence of Snow and Ice Crystal Formation and Accumulation on Mercury Deposition to the Arctic. *Environ. Sci. Technol.* **2008**, *42* (5), 1542–1551. DOI: 10.1021/es070502d.
(34) Kirk, J. L.; St. Louis, V. L.; Sharp, M. J. Rapid Reduction and Reemission of Mercury Deposited into Snowpacks during Atmospheric Mercury Depletion Events at Churchill, Manitoba, Canada. *Environ. Sci. Technol.* **2006**, *40* (24), 7590–7596. DOI: 10.1021/es061299+.
(35) Constant, P.; Poissant, L.; Villemur, R.; Yumvihoze, E.; Lean, D. Fate of Inorganic Mercury and Methyl Mercury within the Snow Cover in the Low Arctic Tundra on the Shore of Hudson Bay (Québec, Canada). *J. Geophys. Res.* **2007**, *112*, D08309. DOI: 10.1029/2006JD007961.
(36) Larose, C.; Dommergue, A.; De Angelis, M.; Cossa, D.; Averty, B.; Marusczak, N.; Soumis, N.; Schneider, D.; Ferrari, C. Springtime Changes in Snow Chemistry Lead to New Insights into Mercury Methylation in the Arctic. *Geochim. Cosmochim. Acta* **2010**, *74* (22), 6263–6275. DOI: 10.1016/j.gca.2010.08.043.
(37) Asaduzzaman, A. Md.; Wang, F.; Schreckenbach, G. Quantum-Chemical Study of the Diffusion of Hg(0, I, II) into the Ice(Ih). *J. Phys. Chem. C* **2012**, *116* (8), 5151–5154. DOI: 10.1021/jp212195w.
(38) Durnford, D.; Dastoor, A. The Behavior of Mercury in the Cryosphere: A Review of What We Know from Observations. *J. Geophys. Res.* **2011**, *116*, D06305. DOI: 10.1029/2010JD014809.
(39) Kresse, G.; Furthmüller, J. Efficiency of Ab-Initio Total Energy Calculations for Metals and Semiconductors Using a Plane-Wave Basis Set. *Comput. Mater. Sci.* **1996**, *6*, 15–50. DOI: 10.1016/0927-0256(96)00008-0.
(40) Kresse, G.; Joubert, D. From Ultrasoft Pseudopotentials to the Projector Augmented-Wave Method. *Phys. Rev. B* **1999**, *59* (3), 1758–1775. DOI: 10.1103/PhysRevB.59.1758.
(41) Perdew, J. P.; Burke, K.; Ernzerhof, M. Generalized Gradient Approximation Made Simple. *Phys. Rev. Lett.* **1996**, *77* (18), 3865–3868. DOI: 10.1103/PhysRevLett.77.3865.
(42) Blöchl, P. E. Projector Augmented-Wave Method. *Phys. Rev. B* **1994**, *50* (24), 17953–17979. DOI: 10.1103/PhysRevB.50.17953.
(43) Armiento, R.; Mattsson, A. E. Functional Designed to Include Surface Effects in Self-Consistent Density Functional Theory. *Phys. Rev. B* **2005**, *72*, 085108. DOI: 10.1103/PhysRevB.72.085108.
(44) Mattsson, A. E.; Armiento, R.; Paier, J.; Kresse, G.; Wills, J. M.; Mattsson, T. R. The AM05 Density Functional Applied to Solids. *J. Chem. Phys.* **2008**, *128*, 084714. DOI: 10.1063/1.2835596.
(45) Mattsson, A. E.; Armiento, R. Implementing and Testing the AM05 Spin Density Functional. *Phys. Rev. B* **2009**, *79*, 155101. DOI: 10.1103/PhysRevB.79.155101.
(46) Perdew, J. P.; Ruzsinszky, A.; Csonka, G. I.; Vydrov, O. A.; Scuseria, G. E.; Constantin, L. A.; Zhou, X.; Burke, K. Restoring the Density-Gradient Expansion for Exchange in Solids and Surfaces. *Phys. Rev. Lett.* **2008**, *100*, 136406. DOI: 10.1103/PhysRevLett.100.136406.

(47) Asaduzzaman, A. M.; Schreckenbach, G. Adsorption of Na and Hg on the Ice(Ih) Surface: A Density-Functional Study. *J. Phys. Chem. C* **2010**, *114* (7), 2941–2946. DOI: 10.1021/jp9073202.
(48) Chen, J.; Schusteritsch, G.; Pickard, C. J.; Salzmann, C. G.; Michaelides, A. Two Dimensional Ice from First Principles: Structures and Phase Transitions. *Phys. Rev. Lett.* **2016**, *116*, 025501. DOI: 10.1103/PhysRevLett.116.025501.
(49) Sun, Z.; Pan, D.; Xu, L.; Wang, E. Role of Proton Ordering in Adsorption Preference of Polar Molecule on Ice Surface. *Proc. Natl. Acad. Sci. USA* **2012**, *109* (33), 13177–13181. DOI: 10.1073/pnas.1206879109.
(50) Asaduzzaman, A. M.; Zega, T. J.; Laref, S.; Runge, K.; Deymier, P. A.; Muralidharan, K. A Computational Investigation of Adsorption of Organics on Mineral Surfaces: Implications for Organics Delivery in the Early Solar System. *Earth Planet Sci. Lett.* **2014**, *408*, 355–361. DOI: 10.1016/j.epsl.2014.10.029.
(51) Bader, R. F. W. *Atoms in Molecules: A Quantum Theory*; The International series of monographs on chemistry; Clarendon Press: Oxford ; New York, 1990.
(52) Henkelman, G.; Arnaldsson, A.; Jónsson, H. A Fast and Robust Algorithm for Bader Decomposition of Charge Density. *Comput. Mater. Sci.* **2006**, *36*, 354–360. DOI: 10.1016/j.commatsci.2005.04.010.
(53) Sanville, E.; Kenny, S. D.; Smith, R.; Henkelman, G. Improved Grid-Based Algorithm for Bader Charge Allocation. *J. Comput. Chem.* **2007**, *28* (5), 899–908. DOI: 10.1002/jcc.20575.
(54) Tang, W.; Sanville, E.; Henkelman, G. A Grid-Based Bader Analysis Algorithm without Lattice Bias. *J. Phys.: Condens. Matter* **2009**, *21*, 084204. DOI: 10.1088/0953-8984/21/8/084204.

TOC Graphic